

## Temperature Dependence of Low Cloud Optical Thickness in the GISS GCM: Contributing Mechanisms and Climate Implications

GEORGE TSELILOUDIS

*Department of Applied Physics, Columbia University, and NASA/Goddard Institute for Space Studies, New York, New York*

ANTHONY D. DELGENIO

*NASA/Goddard Institute for Space Studies, New York, New York*

WILLIAM KOVARI JR.

*Department of Applied Physics, Columbia University, and NASA/Goddard Institute for Space Studies, New York, New York*

MAO-SUNG YAO

*Science Systems Applications Inc., and NASA/Goddard Institute for Space Studies, New York, New York*

(Manuscript received 18 April 1997, in final form 30 September 1997)

### ABSTRACT

A current-climate simulation of the Goddard Institute for Space Studies (GISS) GCM, which includes interactive cloud optical properties that depend on the predicted cloud water content, is analyzed to document the variations of low cloud optical thickness with temperature in the model atmosphere. It is found that low cloud optical thickness decreases with temperature in the warm subtropical and tropical latitudes and increases with temperature in the cold midlatitude regions. This behavior is in agreement with the results of two observational studies that analyzed satellite data from the International Satellite Cloud Climatology Project and Special Sensor Microwave/Imager datasets. The increase of low cloud optical thickness with temperature in the midlatitudes is due to decreases in cloud water content and happens despite increases in cloud vertical extent. The cloud processes that produce the cloud property changes in the model also vary with latitude. In the midlatitude regions relative-humidity-induced increases of cloud vertical extent with temperature dominate, whereas in the Tropics increases in cloud-top entrainment and precipitation with temperature produce decreases of cloud water content, whose effect on optical thickness outweighs the effect of entrainment-induced increases of cloud vertical extent with temperature. Doubled-CO<sub>2</sub> simulations with the GISS GCM suggest that even though low cloud optical thickness changes have little effect on the global climate sensitivity of the model, they redistribute the temperature change and reduce the high-latitude amplification of the greenhouse warming. It is also found that the current-climate variations of low cloud optical thickness with temperature reproduce qualitatively but overestimate quantitatively the changes in optical thickness with climate warming.

### 1. Introduction

Despite recent advances in the representation of clouds in general circulation models (GCMs), the issue of cloud feedbacks on climate remains largely unresolved. Early GCMs that allowed cloud cover and height to vary but prescribed cloud optical properties as a fixed function of altitude produced positive cloud feedbacks due to a shift to higher clouds in a warmer climate (Hansen et al. 1984; Washington and Meehl 1984; Weth-

erald and Manabe 1986). Many new-generation GCMs include interactive cloud optical properties that depend on the predicted cloud water content, and, therefore, can predict cloud optical property feedbacks explicitly (e.g., Smith 1990; Le Treut and Li 1991; Fowler et al. 1995; Del Genio et al. 1996). The cloud optical property feedbacks produced by these GCMs, however, differ among them both in magnitude and in sign (e.g., Roeckner 1988; Mitchell et al. 1989). These differences are due to the fact that, in the models' cloud schemes, cloud optical properties are heavily dependent on the parameterization of cloud-related processes like cloud-top entrainment, the transition from water to ice cloud particles, and the initiation and strength of precipitation (Mitchell et al. 1989; Li and LeTreut 1992). Differences

---

*Corresponding author address:* Dr. George Tselioudis, NASA/Goddard Institute for Space Studies, 2880 Broadway, New York, NY 10025.  
E-mail: gtselioudis@giss.nasa.gov

in the models' parameterizations of those processes result in large differences in the models' climate sensitivity.

The reliability of a GCM's climate predictions is traditionally inferred by the model's ability to simulate the current climate. The main approach to model verification has been to compare model fields averaged in time and/or space to those obtained from observations. Climate sensitivity, however, depends primarily on the sign and strength of feedbacks (e.g., Hansen et al. 1984) that are produced by the response of atmospheric fields to changing atmospheric conditions. It is more appropriate, then, to test a GCM's ability to predict climate change by examining its capability to simulate current-climate changes in atmospheric fields with varying atmospheric conditions. If such changes are similar to those found in observations, this provides additional confidence in the ability of the model fields to respond to climate forcings such as the increase in atmospheric carbon dioxide. This variability based approach to model verification is being followed by some model groups, mostly in relation to a GCM's ability to reproduce diurnal, seasonal, or ENSO-related changes in surface temperature and sea level pressure (e.g., Blackmon et al. 1983). With respect to clouds, however, few efforts have been undertaken to examine the response of model cloud parameters to changing atmospheric conditions. Del Genio et al. (1996) examined diurnal, seasonal, and interannual changes in the Goddard Institute for Space Studies (GISS) GCM cloud properties and compared them with observations from the International Satellite Cloud Climatology Project (ISCCP). They also examined the variation of model cloud properties with temperature and commented on the model performance in comparison to satellite and in situ observations.

The objective of the present work is to diagnose the GISS GCM's cloud field with respect to an observed relationship between low cloud optical thickness and temperature. In two recent papers, Tselioudis et al. (1992, henceforth referred to as TEA92) and Tselioudis and Rossow (1994) analyzed satellite observations from the ISCCP dataset and found that, with the exception of the coldest temperature regimes, the optical thickness of low clouds decreases with cloud temperature. This decrease is in the opposite direction from the thermodynamically expected increase in cloud liquid water content with temperature. When applied to a two-dimensional radiative-convective model, the optical thickness-temperature relation acts to reduce the high-latitude amplification of the model's greenhouse warming (Tselioudis et al. 1993). A similar relationship between cloud liquid water path and cloud temperature was found in an analysis of microwave satellite observations by Greenwald et al. (1995).

In this paper, we will first document the relationship between low cloud optical thickness and cloud temperature in a current-climate simulation with the GISS GCM, and we will compare the behavior of the model

low clouds to that found in the ISCCP data. Then, we will examine the cloud parameters and atmospheric processes that are responsible for the model relationship, and we will use a doubled-CO<sub>2</sub> simulation to explore the climate implications of the cloud optical thickness variations. To the extent that a relationship similar to the observed one exists in the model atmosphere, the analysis of the model fields will allow us to identify cloud properties and atmospheric mechanisms that may be responsible for the observed behavior. Furthermore, the evaluation of the relationship with respect to changes that occur in a climate warming scenario will provide an estimate of the reliability of the use of a current-climate relationship as a surrogate for climate change. Finally the use of the GISS GCM will allow us to examine cloud optical thickness feedbacks in a climate model with fully interactive cloud optical properties.

The second section of the paper is an extended description of the cloud scheme employed in the GISS GCM. In the third section, the variations of the model low cloud optical thickness with cloud temperature are compared to those found in the satellite data, the cloud physical properties that are responsible for those variations are explored, and the physical mechanisms that cause the cloud properties to vary with temperature are discussed. In the fourth section, the feedbacks that low-cloud optical thickness variations produce in a climate warming simulation are examined. Finally, the main points of the paper are summarized and discussed in the fifth section.

## 2. The model

The version of the GISS GCM used for the analysis in this paper is identical to that described in Del Genio et al. (1996). The baseline version of the model has 4° lat × 5° long horizontal resolution and nine vertical layers. Low clouds in the GCM are defined as those whose tops lie in one of the three model layers below the 720-mb level. From the surface upward, these layers have global mean pressure thicknesses of 50, 80, and 134 mb, respectively [see Hansen et al. (1983) for further details].

The prognostic cloud water parameterization used to determine the occurrence, cloud cover, and optical properties of stratiform clouds is described in detail by Del Genio et al. (1996). The salient aspects of that parameterization for the present discussion are as follows: cloud formation and condensation are determined according to the available moisture convergence into the grid box following the approach of Sundqvist et al. (1989), with a threshold relative humidity of 60% specified for stratiform cloud occurrence. The grid box is divided into cloudy and clear fractions; the cloudy part is assumed saturated, and relative humidity in the clear part is assumed to increase linearly as cloud fraction increases, also following Sundqvist et al. (1989). Above

the threshold relative humidity, cloud fraction increases with grid box relative humidity as in Sundqvist (1978).

Statistically, there is evidence from both observations and cloud-resolving models (cf. Walcek 1994; Xu and Krueger 1991) that cloud areal fraction should be an increasing function of relative humidity. However, there is significant scatter in the relationship, indicating that other factors influence cloudiness as well.

Furthermore, the spirit of the Sundqvist approach of moisture convergence into a volume determining cloud occurrence suggests that the cloud fraction it diagnoses should be interpreted as the fraction of the grid box volume occupied by clouds with no a priori assumption about how the box is filled with cloud vertically and horizontally, as opposed to the traditional assumption in GCMs of clouds filling grid boxes vertically and cloud fraction being distributed only horizontally. Indeed, the coarse vertical resolution of climate GCMs is not sufficient in general to resolve typical cloud physical thicknesses, arguing for the need for parameterization of cloud thickness as well as areal fraction.

In this version of the GCM, clouds do not necessarily fill the entire vertical extent of a model layer. The sub-grid physical thickness is parameterized semiempirically as a function of both the layer relative humidity and the moist stability of the layer with respect to the layer above. Specifically, cloud areal fraction is assumed to be identical to the diagnosed cloud volume fraction (i.e., clouds fill the layer vertically) when either moist convection or cloud-top entrainment instability has occurred in the same time step. In stable conditions, however, the cloud areal fraction increases and the physical thickness decreases to less than the thickness of a model layer, thus decreasing the optical thickness as well. Cloud vertical extent can thus change either via a change in the number of layers simultaneously occupied by cloud or by a change in the cloud thickness within a single layer. In the stable case, since there is fractional cloudiness in all three dimensions and cloud volume fraction increases with relative humidity, cloud physical thickness increases with relative humidity; in effect, cloud bases descend as the boundary layer moistens.

Although the parameterization described above cannot be rigorously validated against observations (due to the lack of a suitable global cloud thickness climatology), it is qualitatively consistent with several observed aspects of low cloud behavior: 1) The dependence of cloud areal fraction on stability, via the trade-off with physical thickness, introduces realistic scatter into the model cloud cover–relative humidity relationship; 2) Klein and Hartmann (1993) observed a positive correlation between marine stratus cloud cover and low-level static stability; 3) Albrecht et al. (1995) generally observe cloud thickness to increase between the near-neutral First ISCCP Regional Experiment (FIRE) San Nicholas boundary layer and the conditionally unstable equatorial boundary layer sampled during the Tropical Instability Wave Experiment; 4) Considine et al. (1997)

show that the Landsat-derived dependence of the probability distribution of marine stratus liquid water path on cloud cover can be simply explained by plausible fluctuations of PBL relative humidity and hence lifting condensation level for surface parcels, such that more humid parcels saturate at lower altitudes and produce thicker clouds.

Three parameterized sinks of cloud water content are important for isolated low-level clouds in the GCM: 1) Autoconversion of cloud water into precipitation is parameterized as an increasing function of cloud water content [following Sundqvist et al. (1989) but with an even stronger dependence on cloud water, ensuring significant drizzle in warm PBL clouds] and a weakly decreasing function of vertical velocity, and occurs more readily over ocean than land in recognition of marine-continental aerosol concentration differences. 2) Evaporation of cloud water depends on the cloud water content, the relative humidity and temperature of the air outside the cloud, and the mean cloud droplet size. 3) Drying by entrainment of air into the cloud from the layer above cloud top is parameterized as an increasing function of the ratio of the cloud-top interface jumps in moist static energy and total water content. It is assumed to occur only marginally when this ratio begins to exceed the cloud-top entrainment instability criterion of Randall (1980); complete destruction of the cloud does not occur until the restrictive instability criterion of MacVean and Mason (1990), which is rarely met in either observed or GCM low clouds, is exceeded. The resulting degree of PBL drying and reduction of cloud water by entrainment depends on the humidity of the air above the cloud [an effect observed by Hanson (1991)] as well as the strength of the entrainment.

Visible cloud optical thickness ( $\tau$ ) in a layer is parameterized according to

$$\tau = \frac{3\mu dZ}{2\rho R_e}, \quad (1)$$

where  $\mu$  is the cloud water content,  $dZ$  the cloud physical thickness,  $\rho$  the density of liquid water, and  $R_e$  the effective radius of the droplet size distribution. Effective radius is based on an assumed constant number concentration of cloud droplets (greater over land than ocean, and less for ice than for liquid clouds) and scales as  $\mu^{1/3}$ . Effective radius is not allowed to increase beyond an upper limit consistent with the threshold cloud water content for efficient autoconversion. Fractional cloudiness in space is converted to an effective fractional cloudiness in time by the GCM radiation calculation, via a comparison of layer cloud areal fraction with a random number and subsequent assignment of either zero or total cloud cover. For comparison with ISCCP, which detects only the column optical thickness of low clouds with no other clouds above them, we “detect” low clouds in the GCM as those with tops in the first three layers and no higher cloud layers simul-

taneously present. The column optical thickness is then simply the sum of the optical thicknesses of all clouds in the three layers that survive the random number comparison. The distribution of optical thicknesses in different climate regimes in the GCM compares reasonably well with that observed by ISCCP [cf. Figs. 14–16 of Del Genio et al. (1996) as well as other figures and discussion in that paper documenting the simulation of model cloud cover, cloud forcing, and cloud liquid water path].

Shallow cumulus clouds with specified optical thicknesses are also predicted by the GCM's mass flux cumulus parameterization (Del Genio and Yao 1993), which allows for both entraining and nonentraining plumes at the same time and location. Both deep and shallow cumulus are predicted by the same scheme; shallow cumulus are defined as those whose level of vanishing buoyancy occurs in either the second or third model layer above the surface. In general, shallow cumulus occurrence is underpredicted by the current scheme, and these clouds do not appear to control any of the behavior reported in this paper.

This version of the GISS GCM uses a simple boundary layer parameterization described originally in Hansen et al. (1983) that has been modified by Hartke and Rind (1997). A drag law parameterization computes momentum, heat, and moisture fluxes from the ground into a surface air layer; similarity theory is used to specify the instability functions that determine the drag coefficient, Stanton number, and Dalton number. The surface layer is assumed to be in thermodynamic equilibrium; that is, the fluxes from the ground are equated to diffusive fluxes from the surface layer to the first model layer, with turbulent transport coefficients and the height of the base of the mixed layer also computed from similarity theory (this determines the surface temperature and humidity). Surface roughness, which affects the neutral surface drag and transfer coefficients, depends on the standard deviation of topography and vegetation over land, and on surface momentum flux over ocean. The surface wind is interpolated from that at the top of the PBL using a modified Ekman model with constant turbulent viscosity solved on a finite domain. Dry convective adjustment subsequently mixes properties from the first model layer to higher layers. The highest model layer to which dry convection penetrates is defined as the PBL top; over land this may at times be as high as layer three, but over ocean the thickness of the first layer is comparable to the typical depth of the PBL and dry convection to higher levels occurs only rarely. The evaporative and sensible heat fluxes produced by the PBL scheme influence the global distribution of low-level relative humidity and stability and thus are crucial to the occurrence and optical properties of the PBL clouds in the model. However, recent experiments replacing the operational PBL scheme with a second-order closure model produce very similar low-level cloud distributions and shortwave cloud forcing in the GCM. It there-

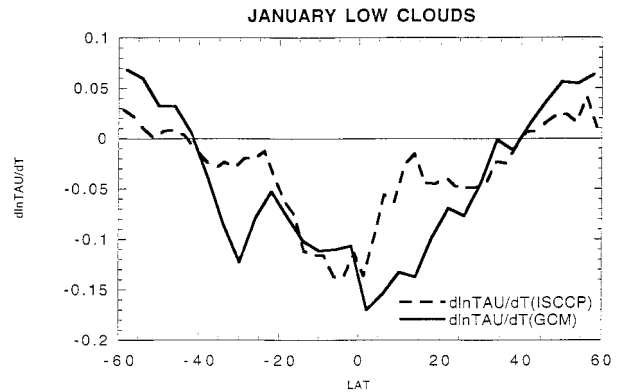


FIG. 1. Latitudinal distribution of the logarithmic derivative of low cloud optical thickness with temperature [ $d \ln(\text{TAU})/dT$ ] for January, from a GCM control simulation (solid line) and from ISCCP data (dashed line).

fore appears that the behavior described in this paper is most sensitive to choices made in the stratiform cloud parameterization (which computes entrainment fluxes into the PBL in the presence of cloud) and does not depend on the other details of the GISS PBL representation itself.

### 3. Low cloud optical thickness variations with temperature

#### a. The cloud optical thickness–temperature relation

A January current-climate simulation with the GISS GCM is analyzed to document the variations of low cloud optical thickness with temperature in the model atmosphere. The analysis method is similar to the one used in TEA92: for each latitude and for the whole month, the 3-h gridbox values of low cloud optical thickness (TAU) and low cloud temperature ( $T$ ) are used to derive the logarithmic derivative of optical thickness with temperature [ $d \ln(\text{TAU})/dT$ ]. Low cloud optical thickness is defined as the column optical thickness when the highest cloud in the grid box occurs in layer three or lower, whereas low cloud temperature is the mean temperature of the first three layers when a low cloud is present. The definition of low cloud differs slightly from the one used in TEA92, since in the ISCCP the upper bound for low cloud tops is 680 mb whereas in the model it is 720 mb.

The variation of  $d \ln(\text{TAU})/dT$  with latitude in the model clouds is shown in Fig. 1, along with the same parameter for a composite of seven Januaries from the ISCCP observations. It can be seen that the two  $d \ln(\text{TAU})/dT$  curves exhibit similar characteristics: positive values are found only at the highest latitudes, the transition to negative values happens near  $40^\circ$  in both hemispheres, and the values of the negative peak in the Tropics are near  $-0.15$ . The only differences are related to the fact that model low clouds show sharper increases of optical thickness with temperature in the

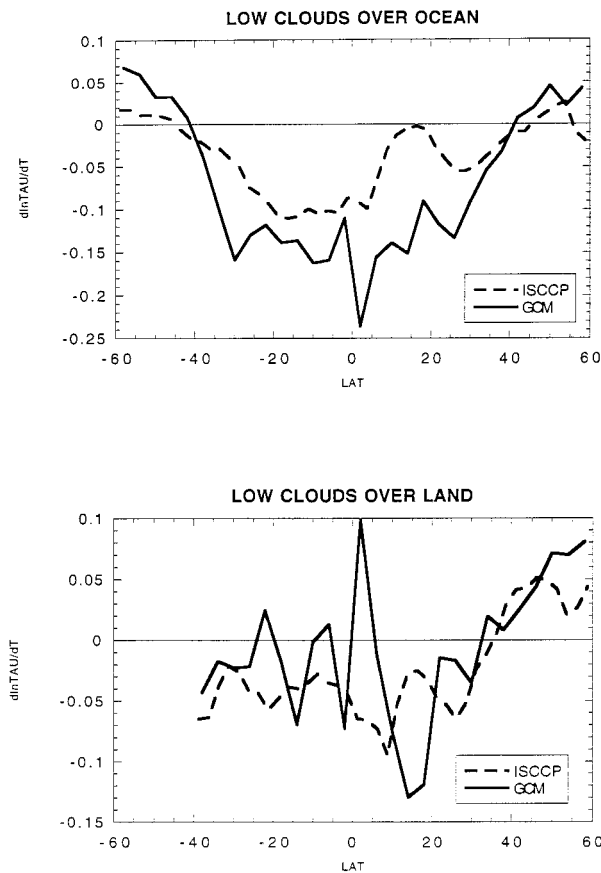


FIG. 2. As in Fig. 1 but for clouds over ocean (top) and clouds over land (bottom).

high latitudes and sharper decreases in the subtropics than those found in the ISCCP data. Overall, however, the model low clouds capture the observed behavior that calls for increases of optical thickness with temperature in the cold high-latitude regimes and decreases of optical thickness with temperature everywhere else.

To explore the differences in low cloud optical thickness behavior between clouds located over land and ocean regions, the latitudinal variation of  $d \ln(\text{TAU})/dT$  for maritime and continental clouds is plotted in Fig. 2 for both the GCM output and the ISCCP dataset. It can be seen that while maritime low clouds (Fig. 2, top) in the model exhibit similar behavior to the observed (with the caveats mentioned above), continental low clouds (Fig. 2, bottom) show erratic variations of  $d \ln(\text{TAU})/dT$ , particularly in latitudes south of 20°N. This behavior can be attributed to the latitudinal variation of the number of data points that go into calculating  $d \ln(\text{TAU})/dT$  (Fig. 3, top). Over ocean, consistently more than 1000 data points per latitude enter the calculation producing statistically significant correlations [ $d \ln(\text{TAU})/dT$  values greater (less) than 0.02 (−0.04) are significant at the 99% level when the number of observations exceeds 1000], whereas over land the number of data points is below 500 in latitudes south of 20°N, making

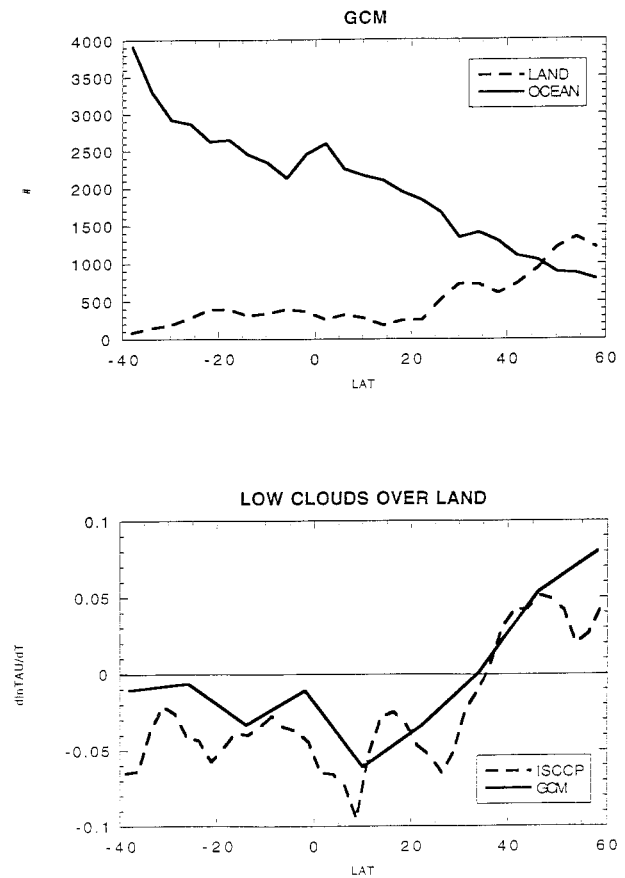


FIG. 3. (top) Number of low cloud observations over ocean (solid line) and over land (dashed line), from a January control simulation of the GISS GCM. (bottom) As in Fig. 2, bottom panel, but for GCM  $d \ln(\text{TAU})/dT$  values calculated over 12° latitude zones.

the statistical significance of the  $d \ln(\text{TAU})/dT$  calculations very low. To increase the statistical significance of the  $d \ln(\text{TAU})/dT$  calculations over land, we degrade the 4° model resolution and calculate  $d \ln(\text{TAU})/dT$  values over 12°-wide latitude zones. When this is done (Fig. 3, bottom), the resulting cloud optical thickness variations resemble the ones found in the ISCCP observations. Nevertheless, the dominance of maritime clouds in the low cloud field illustrated in Fig. 3 (top) together with their realistic latitudinal variation of  $d \ln(\text{TAU})/dT$  shown in Fig. 2 (top), makes such clouds the perfect candidate to explore the mechanisms responsible for the observed optical thickness behavior. Therefore, the analysis of the model clouds presented below will concentrate primarily to maritime low clouds.

The zonal-mean  $d \ln(\text{TAU})/dT$  values shown in Fig. 2 (top) are derived using January instantaneous TAU and  $T$  data from all the maritime grid boxes at each latitude circle. This implies that those values can be due either to time variations of the two quantities in each grid box or to persistent longitudinal contrasts in the quantities. To explore this issue local values of  $d \ln(\text{TAU})/dT$  were calculated at each latitude circle,

using grid boxes with longitudinal extents of  $90^\circ$ ,  $45^\circ$ , and  $22.5^\circ$  for ISCCP and  $90^\circ$ ,  $60^\circ$ , and  $30^\circ$  for the GCM. In the midlatitude regions, both the observations and the model showed positive TAU– $T$  correlations down to the smallest local scale. In the southern midlatitudes most of those correlations were statistically significant, whereas in the northern midlatitudes few of the positive correlations were above the 95% significance level. In the subtropics, the negative  $d \ln(\text{TAU})/dT$  values were dominant down to the  $45^\circ$  scale in the observations and the  $60^\circ$  scale in the model; in the smallest scale examined, significantly more negative than positive correlations were found in both the observations and the model, and this difference became even more pronounced when only statistically significant correlations were counted. In the Tropics, the observations showed more negative correlations in the  $45^\circ$  scale but also an area of positive correlations near Indonesia and the western part of the Pacific warm pool. In the  $22.5^\circ$  scale a mix of positive and negative correlations was found, but when only statistically significant correlations were considered almost all of them were negative. The GCM showed similar behavior with the observations in the Tropics, with somewhat larger numbers of negative correlations in the two smallest scales and with no area of positive correlations in the western Pacific. Overall it can be said that, both in the observations and in the model, the midlatitude and subtropical zonal-mean TAU– $T$  correlations retain their sign down to the local scale; in the Tropics, where local temperature variations in the period of a month are very small, local TAU– $T$  correlations are both positive and negative and, for the most part, are not statistically significant. The few tropical correlations that exceed the 95% significance level are almost all negative.

As mentioned in the beginning of the section, the presence of a low cloud in the model implies that the cloud top (i.e., the highest cloud layer) in the grid box is one of the three lowest layers. To separate the contribution to the low cloud optical thickness variations of clouds with different cloud tops, the latitudinal variation of  $d \ln(\text{TAU})/dT$  for clouds with tops in layers one, two, and three are plotted in Fig. 4 (top). All three cloud types show similar cloud optical thickness behavior resembling the one observed for all low clouds (Fig. 2, top). However, with the exception of the northern midlatitudes, layer 1 contains more low cloud tops than layers 2 or 3 (Fig. 4, bottom). This, along with the observation that  $d \ln(\text{TAU})/dT$  variations in any single layer are representative of the overall low cloud behavior, and the fact that in single-layer clouds it is easier to attribute changes in cloud parameters to processes operating within the layer, makes it practical to use layer-one-top clouds to study the cloud properties and processes responsible for the optical thickness changes with temperature. The analysis will extend to clouds with tops in layers two and three, and any significant differences with the layer-one-top clouds will be discussed.

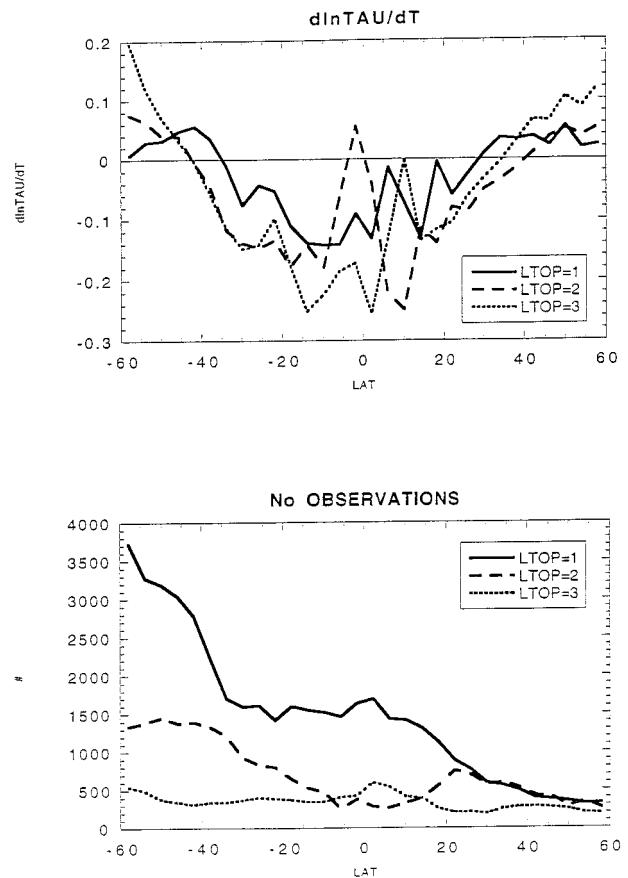


FIG. 4. (top) Latitudinal distribution of  $d \ln(\text{TAU})/dT$  from a January simulation of the GISS GCM for ocean clouds with tops in layer 1 (solid line), layer 2 (dashed line), and layer 3 (dotted line). (bottom) Number of low cloud observations for ocean clouds with tops in layer 1 (solid line), layer 2 (dashed line), and layer 3 (dotted line).

#### b. Cloud parameters responsible for the optical thickness–temperature relation

Cloud optical thickness, both in the model and in the real world, is proportional to the liquid water content (LWC) and the vertical extent (DZ) of the cloud, and inversely proportional to the effective radius of the cloud particle size distribution ( $R_e$ ) [see Eq. (1), also Hansen and Travis (1974) and Del Genio et al. (1996)]. To examine the relationships between low cloud optical thickness and the cloud physical parameters that explain it, Fig. 5 shows the logarithmic derivatives of cloud optical thickness with LWC (top), DZ (middle), and effective particle radius (bottom) for layer-one-top clouds. Cloud optical thickness is positively correlated with liquid water content, with the highest correlations occurring in the tropical belt. Cloud optical thickness and cloud vertical extent are positively correlated in the midlatitude regions but negatively correlated in the Tropics. Finally, cloud optical thickness is positively correlated everywhere with cloud particle size. This implies that although in the midlatitudes cloud optical

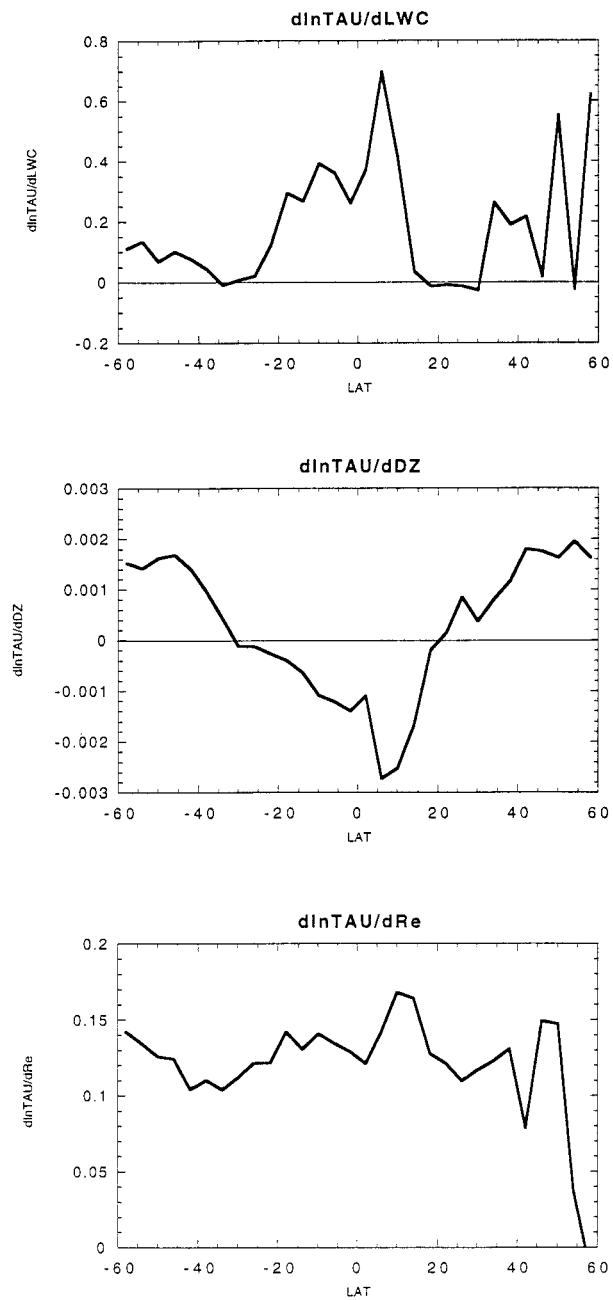


FIG. 5. Latitudinal distributions of the logarithmic derivative of cloud optical thickness with LWC [ $d \ln(\text{TAU})/d\text{LWC}$ ] (top), DZ [ $d \ln(\text{TAU})/d\text{DZ}$ ] (middle), and effective particle radius [ $d \ln(\text{TAU})/dR_e$ ] (bottom), for layer-one-top GCM clouds over ocean.

thickness varies because of changes in DZ and LWC (and despite changes in cloud particle size), in the Tropics cloud optical thickness varies because of changes in LWC and despite changes in DZ and particle size. The positive correlation between optical thickness and particle size is easily explainable: over oceans, since cloud condensation nucleus concentration in the model is constant, cloud particle size varies as  $\text{LWC}^{1/3}$ , whereas

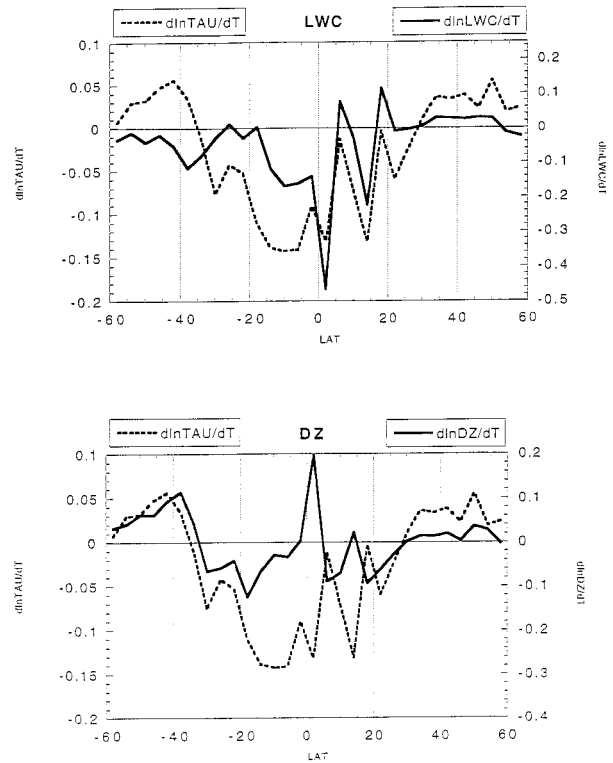


FIG. 6. Latitudinal distribution of  $d \ln(\text{TAU})/dT$  along with  $d \ln(\text{LWC})/dT$  (top) and  $d \ln(\text{DZ})/dT$  (bottom), for layer-one-top GCM clouds over ocean.

cloud optical thickness varies as  $\text{LWC}/R_e$  and hence as  $\text{LWC}^{2/3}$ . Thus, clouds with larger particles have larger water contents, and the latter controls the sign of optical thickness changes. The contrasting behavior between cloud optical thickness and vertical extent in the tropical belt, however, requires further investigation.

To examine the relationships between the temperature dependence of cloud optical thickness, LWC, and DZ,  $d \ln(\text{TAU})/dT$  is plotted in Fig. 6 alongside the logarithmic temperature derivatives of LWC (top) and DZ (bottom). In the midlatitude and subtropical regions  $d \ln(\text{TAU})/dT$  varies coherently with  $d \ln(\text{DZ})/dT$  but in the Tropics those two quantities are anticorrelated. At the same time,  $d \ln(\text{TAU})/dT$  shows little coherence with  $d \ln(\text{LWC})/dT$  in the midlatitudes but varies coherently with it in the Tropics. This is in agreement with the results presented in Fig. 5, and implies that 1) in the midlatitude regions the optical thickness of layer-one-top clouds increases with temperature due to temperature-induced increases in cloud vertical extent, and 2) in the Tropics optical thickness decreases with temperature because of temperature-induced decreases in cloud water content and despite the fact that vertical extent either increases or changes little with temperature. In the subtropics optical thickness decreases with temperature seemingly due to decreases of cloud vertical extent. The subtropical  $d \ln(\text{TAU})/dT$  values, however, are

generally very close to  $-0.04$ , which makes doubtful their statistical significance. The analysis presented above was also performed on clouds with tops in layers two and three: the results were very similar to the ones for layer-one clouds, implying that these conclusions can be extended to all model low clouds.

*c. Atmospheric processes responsible for the cloud parameter variations*

The water content of stratiform clouds in the GCM can change primarily due to changes in the layer relative humidity (RH, which influences the amount of condensate that forms in the grid box), changes in the cloud-top entrainment parameter (CTEIK, which determines the fraction of cloud water that dissipates due to entrainment of dry air at cloud top), and changes in precipitation (PRCP, which in layer-one-top clouds depletes cloud water by forming rain that reaches the ground). Cloud water evaporation also influences the water content of the cloud. Since it operates under similar conditions as cloud-top entrainment, CTEIK will be used to indicate the effects of both cloud water evaporation and cloud-top entrainment on cloud water content.

The relationships between layer-one-top LWC and the processes that affect it are examined in Fig. 7, where the correlation coefficients for  $d \ln(\text{LWC})/d\text{CTEIK}$  (top),  $d \ln(\text{LWC})/d\text{PRCP}$  (middle), and  $d \ln(\text{LWC})/d\text{RH}$  (bottom), are plotted. It can be seen that in the tropical-subtropical zone ( $30^{\circ}\text{S}$ – $30^{\circ}\text{N}$ ) cloud water content depends first on cloud-top entrainment (with 35%–50% of LWC variations explained by CTEIK), second on precipitation (with 3%–8% of the LWC variations explained by PRCP), and shows only marginally significant correlations with relative humidity (a correlation coefficient value of 0.13 or above denotes significance at the 99% level). The relation between the temperature dependence of cloud water content and those of cloud-top entrainment and precipitation are explored in Fig. 8, where  $d \ln(\text{LWC})/dT$  is plotted along with  $d \ln(\text{CTEIK})/dT$  (top) and  $d \text{PRCP}/dT$  (bottom). An increase in CTEIK with temperature near the equator (top panel) coincides with large temperature-induced decreases in LWC. Furthermore, an increase in precipitation with temperature throughout the tropical-subtropical zone coincides with an overall decrease in LWC with temperature. Thus, model oceanic low clouds in the Tropics become optically thinner with warming because they drizzle more and are increasingly diluted by entrainment at warmer temperatures. This behavior occurs despite increasing cloud vertical extent with warming (Fig. 6), which by itself would cause clouds to become optically thicker as temperature rises.

The vertical extent of stratiform clouds in the GCM can change due to changes in RH (under stable conditions, the fraction of the grid-box volume occupied by cloud and thus its depth increase with RH), or due to the occurrence of cloud-top entrainment (the stronger

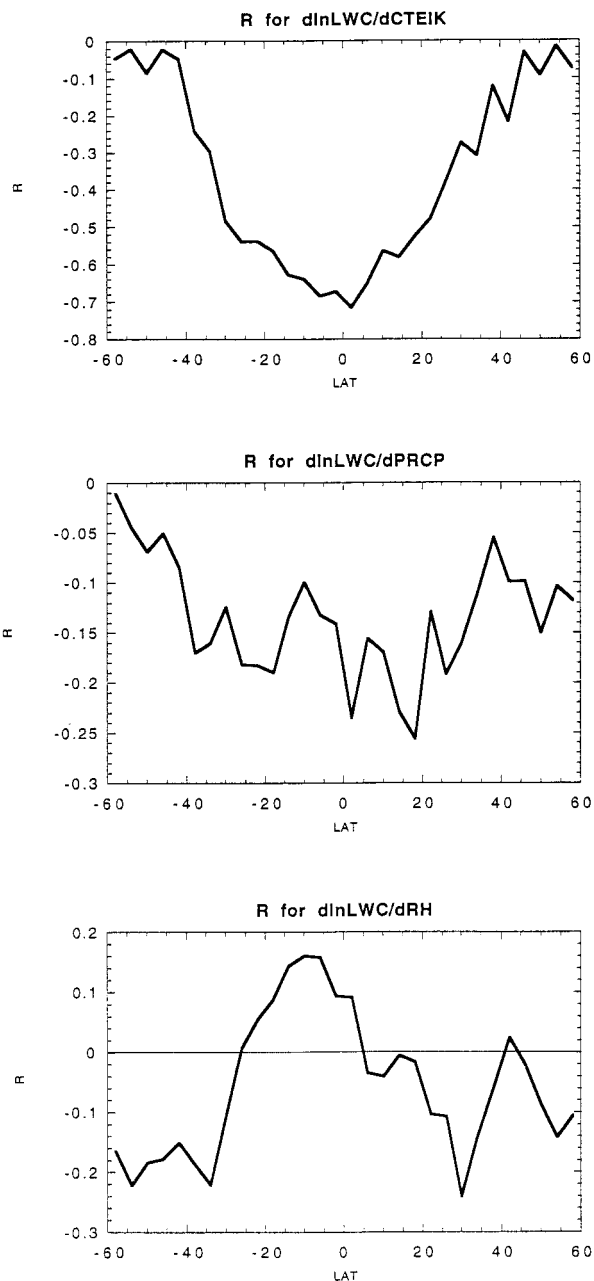


FIG. 7. Correlation coefficients of the logarithmic derivative of LWC with cloud-top entrainment instability [ $d \ln(\text{LWC})/d\text{CTEIK}$ ] (top), precipitation [ $d \ln(\text{LWC})/d\text{PRCP}$ ] (middle), and RH [ $d \ln(\text{LWC})/d\text{RH}$ ] (bottom), for layer-one-top GCM clouds over ocean.

the mixing, the more the cloud fills the grid box vertically) and the occurrence of convection (same effect, but very rare in the case of low-level clouds discussed here). The justification for those dependencies is given in section 2.

The relationships between layer-one-top cloud vertical extent and the processes that affect it are shown in Fig. 9, where the correlation coefficients for  $d \ln(\text{DZ})/$

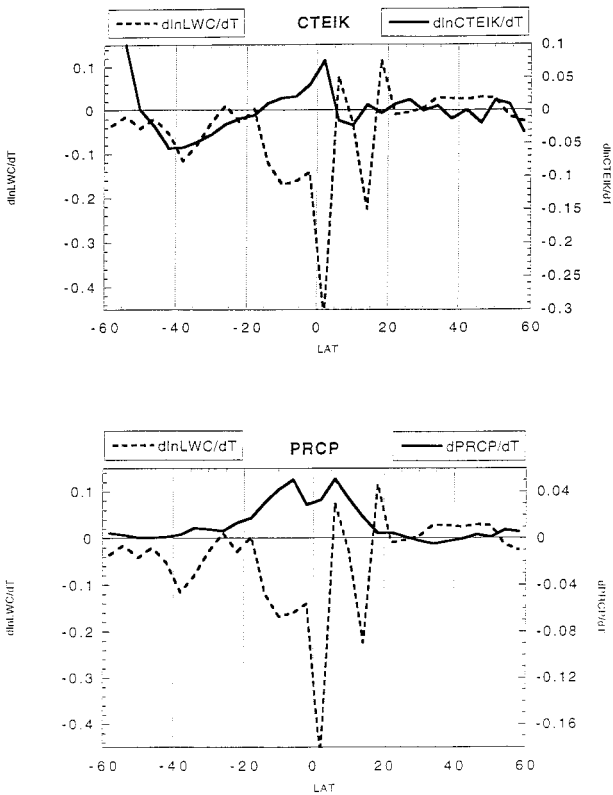


FIG. 8. Latitudinal distribution of  $d \ln(LWC)/dT$  along with  $d \ln(CTEIK)/dT$  (top) and  $d \ln(PRCP)/dT$  (bottom), for layer-one-top GCM clouds over ocean.

$d \ln(CTEIK)/dT$  (top), and  $d \ln(DZ)/dRH$  (bottom), are plotted. In the tropical–subtropical zone DZ is strongly dependent on the CTEIK with the correlation coefficients reaching as high as 0.8. Relative humidity is strongly and positively correlated with DZ in the midlatitude regions, but the two quantities show only weak negative correlations in the Tropics. The temperature dependence of DZ is compared to those of the CTEIK and RH in Fig. 10. Cloud vertical extent changes coherently with cloud-top entrainment in the Tropics and with RH in the midlatitude regions. Thus, in midlatitudes where, for example, more humid air exists in the warm sector of a synoptic wave than behind the cold front, clouds in the warm region are thicker. In the Tropics, clouds thicken as the stability of the top of the PBL erodes with warming; this behavior of model stratiform clouds probably mimics the real-world behavior of trade cumulus, which are underpredicted in the GCM.

An attempt was made to extend the correlative analysis between cloud property and cloud process changes to clouds with tops in layers two and three. The derived correlations in most cases agreed with the layer-one-top results, but in almost all cases lacked statistical significance. This is partly due to the fact that at most latitudes the number of layer-two and layer-three top clouds is small (Fig. 4). It may also be because relating cloud

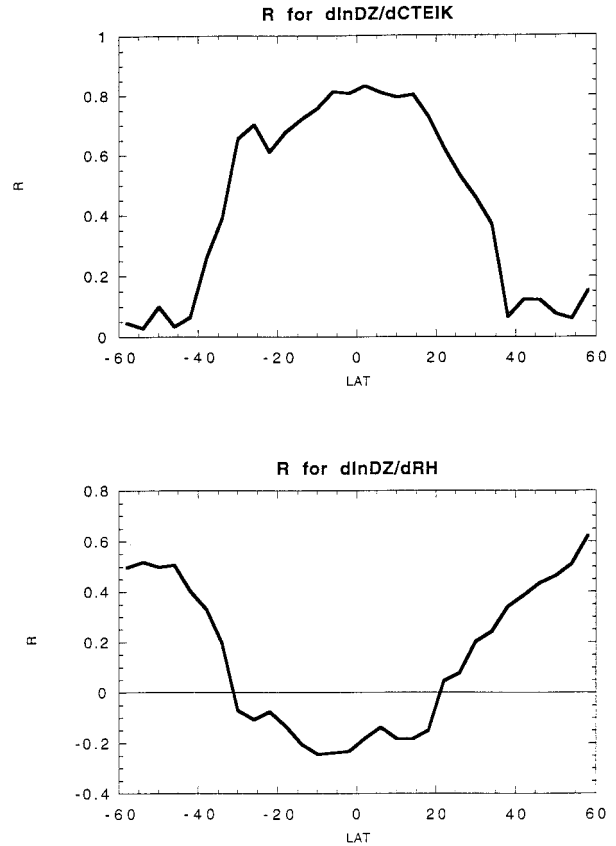


FIG. 9. Correlation coefficients of the logarithmic derivative of DZ with cloud-top entrainment instability [ $d \ln(LWC)/dCTEIK$ ] (top), precipitation [ $(d \ln(LWC)/dPRCP)$ ] (middle), and RH [ $d \ln(LWC)/dRH$ ] (bottom), for layer-one-top GCM clouds over ocean.

properties to processes in multilayered clouds is a more complicated issue. First, the mean properties of the total cloud must be calculated taking into account the relative extent of the cloud in each layer. Then, the effect of each process on the total cloud must be derived as the cumulative effect of the processes operating in each layer. For instance, in the presence of a multilayered cloud, rainfall on the ground is no longer indicative of the effects of precipitation on the cloud properties because precipitation falling into each layer and its re-evaporation rate must be taken into account. Still, the dominance in the total low cloud field of layer-one-top clouds (Fig. 4, bottom), along with the fact that the optical thickness and cloud parameter changes with temperature are similar for clouds of all three cloud tops, indicate that the relationships explored in this section play the major role in determining the temperature behavior of the model low cloud field.

To explain the optical thickness variations with temperature in continental low clouds (Fig. 3, bottom), correlation statistics were calculated between the optical thickness, LWC, and DZ of those clouds. The statistics were obtained over  $12^\circ$  latitude zones to collect enough points for statistically significant correlations. It was

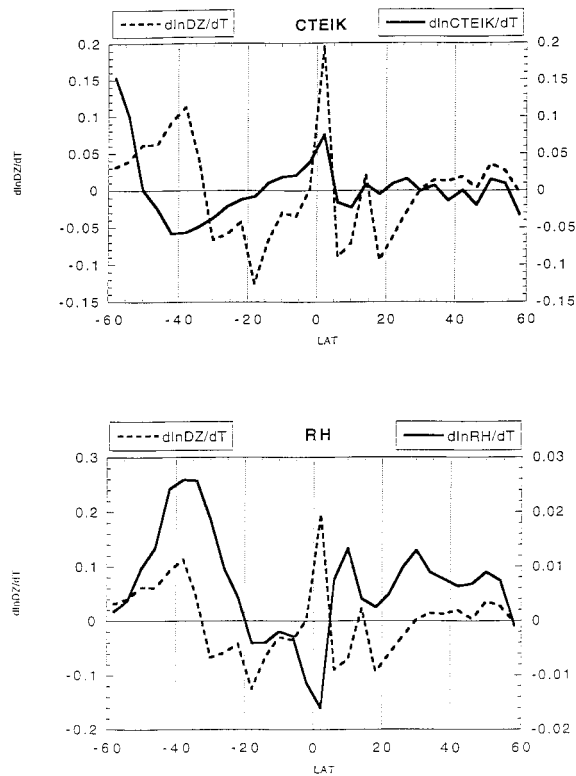


FIG. 10. Latitudinal distribution of  $d \ln(DZ)/dT$  along with  $d \ln(CTEIK)/dT$  (top) and  $d \ln(RH)/dT$  (bottom), for layer-one-top GCM clouds over ocean.

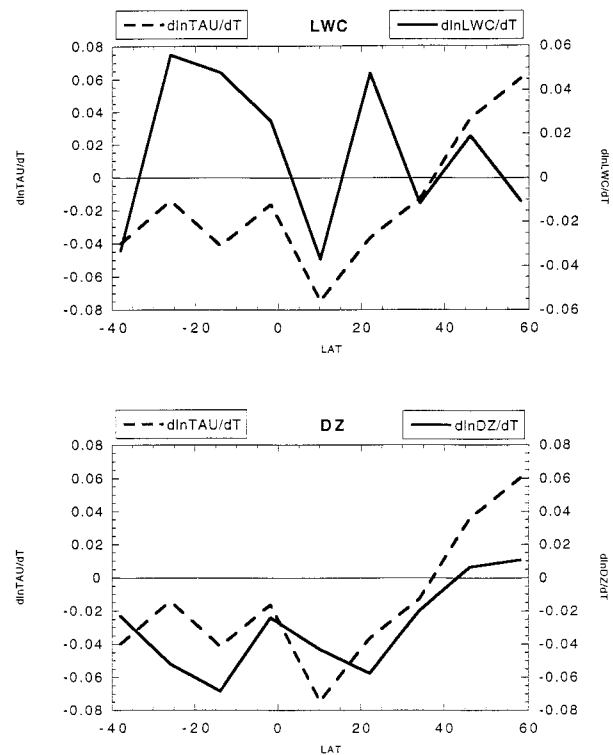


FIG. 11. As in Fig. 6 but for continental layer-one-top GCM clouds.

found that low cloud optical thickness variations over land are explained almost exclusively by changes in DZ. The relationship between the temperature dependence of cloud optical thickness, and LWC and DZ in continental low clouds is shown in Fig. 11, where  $d \ln(TAU)/dT$  is plotted alongside the logarithmic temperature derivatives of LWC (top) and DZ (bottom). It can be seen that the temperature behavior of cloud optical thickness is well correlated with that of DZ but shows little relation with the temperature behavior of LWC.

**4. Low cloud optical thickness feedbacks on climate warming**

The analysis of the GISS GCM current-climate simulation presented in the previous section shows that the model low clouds exhibit optical property variations with temperature similar to the ones found in the ISCCP observations (Fig. 1). These variations are partly due to RH changes with temperature, but depend mostly on changes with temperature in the efficiency of cloud-depleting processes, namely, precipitation and cloud-top entrainment. The first question that arises is whether the current-climate temperature dependence of cloud optical thickness is indicative of how the optical thickness of low clouds will change in a warmer climate. To explore this question, an equilibrium doubled- $CO_2$  simulation

with the same version of the GISS GCM coupled to a mixed layer ocean model with fixed ocean heat transports was run. The model was run for 40 yr, results from the last 10 Januaries (by which time the model had reached equilibrium) were averaged, and those were compared to the current-climate simulation. Figure 12 (top) shows the change in low cloud optical thickness between the  $2 \times CO_2$  and the control runs, along with the logarithmic change with temperature of low cloud optical thickness from the control run. It can be seen that, in a qualitative sense, low cloud optical thickness in the warmer climate changes according to its current-climate temperature dependence: it increases in the mid-latitudes where  $d \ln(TAU)/dT$  is positive and generally decreases in the tropical-subtropical zone where  $d \ln(TAU)/dT$  is negative. To quantify the usefulness of the current-climate optical thickness variations as a climate change predictor, a simple calculation was made that uses the current-climate values of  $d \ln(TAU)/dT$  and the temperature change from the  $2 \times CO_2$  run to predict the cloud optical thickness changes in the warmer climate. Those predicted changes are plotted in Fig. 12 (bottom) along with the actual change in low cloud optical thickness between the  $2 \times CO_2$  and the control runs. The curves show that the prediction based on the current-climate  $d \ln(TAU)/dT$  values captures the qualitative changes in low cloud optical thickness with climate but overestimates those changes by amounts that

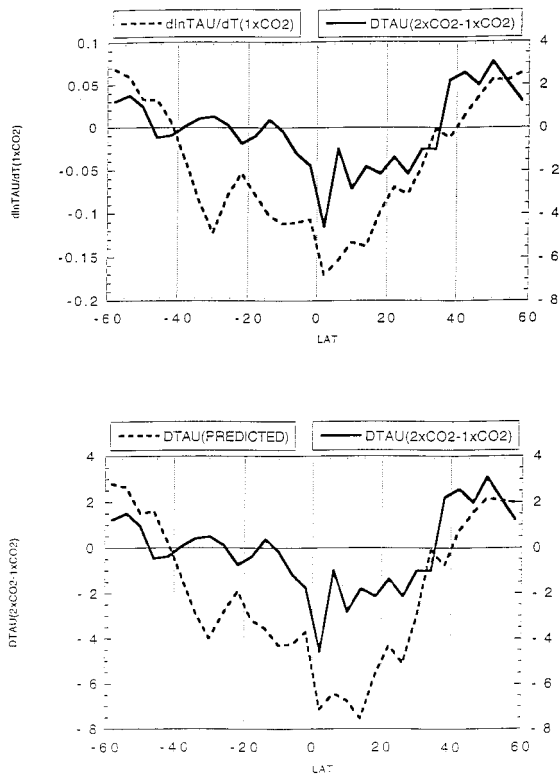


FIG. 12. Latitudinal distribution of the change in low cloud optical thickness between a  $2 \times \text{CO}_2$  and a control run with the GISS GCM (solid line), along with the  $d \ln(\text{TAU})/dT$  curve for the control run (dashed line, top), and the change in optical thickness that is predicted for the warmer climate when the control-run  $d \ln(\text{TAU})/dT$  values are used (dashed line, bottom).

range between 50% and 200%. This does not apply to the midlatitude increases in low cloud optical thickness, where the  $d \ln(\text{TAU})/dT$ -based prediction agrees well with the model-simulated change.

The temperature behavior of low cloud optical thickness in the current-climate and  $2 \times \text{CO}_2$  simulations is presented in Fig. 13. Their similarity implies that the cloud parameters and processes producing that behavior in the model's current-climate simulation are operating in the same manner in the warmer climate run. This similarity suggests that the differences between the thermodynamically predicted and the model-produced optical thickness changes with climate (Fig. 12, bottom) are due to atmospheric dynamics influences on cloud optical thickness, such as climate regime and weather-related variability.

To calculate the feedbacks on the surface temperature that are produced by changes in the optical thickness of low clouds, an additional doubled- $\text{CO}_2$  equilibrium simulation with the GISS GCM was run, where the optical thicknesses of low clouds were specified, as in the older version of the model, as a decreasing function of altitude (cf. Hansen et al. 1983). The latitudinal profile of the surface temperature increase for this run is plotted in Fig. 14, along with the same profile for the  $2 \times \text{CO}_2$

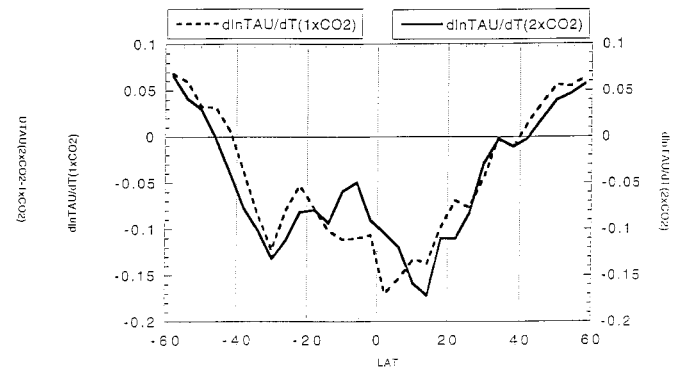


FIG. 13. Latitudinal distributions of  $d \ln(\text{TAU})/dT$  for the control and  $2 \times \text{CO}_2$  runs with the GISS GCM.

run with the fully interactive low cloud optical properties. The two runs have very similar global sensitivities ( $3.1^\circ\text{C}$  for the standard prognostic cloud water version,  $3.0^\circ\text{C}$  for the version with fixed low cloud optical thicknesses) for two reasons: 1) the inclusion in the model of the low cloud optical thickness feedback decreases the greenhouse warming in the higher latitudes and increases it in the Tropics, producing compensating effects on global sensitivity; 2) with fixed (but vertically decreasing) low cloud optical thicknesses, upward shifts in mean cloud height with warming slightly reduce column optical thickness in any case. The contrasting behavior with latitude, however, has a noticeable effect on the high-latitude amplification of the greenhouse warming, decreasing it by about 40% in the Southern Hemisphere and by about 20% in the Northern Hemisphere. This result is in qualitative agreement with the radiative-convective model calculations of Tselioudis et al. (1993).

The regional patterns of greenhouse warming did not show consistent differences between the two runs mentioned in the previous paragraph. For example, although the standard prognostic cloud water run had less warm-

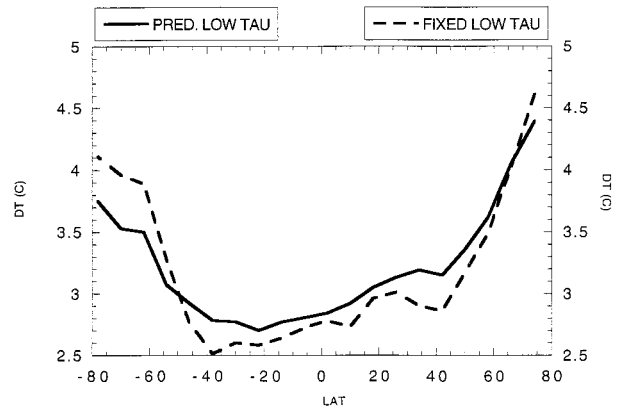


FIG. 14. Latitudinal distributions of the surface temperature change for two  $2 \times \text{CO}_2$  runs, one with predicted (solid line) and the other with fixed (dashed line) low cloud optical thicknesses.

ing than the fixed low cloud optical thickness run in the California and Peru stratocumulus regions, it had more warming in the stratocumulus regions off the coasts of Africa and Australia. It is in the zonal-mean scale that the greenhouse warming of the two runs shows consistent differences.

## 5. Discussion

An analysis of a January current-climate simulation of the GISS GCM showed that the optical thickness of the model low clouds decreases with temperature in the warm subtropical and tropical latitudes and increases with temperature in the cold midlatitude regions. This behavior is in agreement with the results of two observational studies that analyzed satellite data from the ISCCP and SSM/I datasets, implying that the model cloud parameterization reproduces successfully a behavioral aspect of the observed cloud field. The parameterization does not include any explicit dependencies of cloud properties on temperature. It predicts cloud water content following the Sundqvist et al. (1989) approach and depletes cloud water through precipitation and entrainment processes. Furthermore, it allows for sublayer variations of cloud vertical extent, forming clouds that are more vertically developed in unstable environments and more horizontally developed in stable environments.

It was found that over oceans, the increases of optical thickness with temperature in the middle latitudes are due primarily to vertical extent and secondarily to water content increases with temperature, whereas the decreases with temperature in the warm latitudes are due to decreases in water content and happen despite increases with temperature in vertical extent. The decreases of maritime cloud water content with temperature in the warm latitudes appear contradictory to observations of continental clouds over the former Soviet Union (Feigelson 1978), which call for increasing cloud water with temperature (even though they hint of a decrease at the warmest ranges that they cover). Recent observations of summertime high-latitude marine stratus clouds (Gultepe et al. 1996), however, show decreases in water content with temperature throughout the temperature range in which those clouds occur. When the marine stratus observations are combined with the ones of the colder clouds over the former Soviet Union (Fig. 12 of Gultepe et al. 1996), it can be seen that for temperatures greater than 0°C cloud water content generally decreases with temperature. *It is at such temperatures that most of the world's low clouds and all tropical low clouds occur.* This means that the model decreases of low cloud water content with temperature in the warm latitudes are supported by the limited number of available observations. Such decreases are also contrary to the prediction of adiabatic calculations (Betts and Harshvardhan 1987), which call for increasing cloud water with temperature with only a leveling of that increase at the

warmest temperatures. This implies that the observed and the model cloud water decreases over oceans are due to the action of nonadiabatic processes that deplete cloud water, as was originally suggested by TEA92.

An analysis was performed to determine the cloud processes that produce the cloud property changes with temperature in the GCM. In the middle latitudes, DZ increases with temperature because relative humidity increases with temperature. This, physically, is equivalent to the descent of cloud base as the boundary layer moistens. In the Tropics, the decreases in cloud water content with temperature happen because of increases with temperature in the efficiency of precipitation and cloud-top entrainment, two processes that deplete cloud water. Precipitation increases with temperature because the rate of condensation increases with temperature and autoconversion in the model is an increasing function of the amount of condensate. Cloud-top entrainment is parameterized as a function of the potential temperature and moisture contrast between the cloud and the above-cloud layer, and increases with temperature as this contrast increases. This is in agreement with current ideas about the stratocumulus-trade cumulus transition, although there is controversy about the mechanism that accomplishes this transition. It is important to emphasize again here that the low-latitude decreases of cloud optical thickness with temperature happen *despite* the fact that DZs, driven by decreasing stability, become larger over warmer waters. In other words, the novel treatment of DZ in this GCM not only does not produce the optical thickness decreases with temperature in the Tropics but opposes and lessens those decreases.

It is difficult to determine how realistic the cloud property–cloud process relations suggested by the model are. Cloud properties like vertical extent and water content are not routinely measured on large spatial and temporal scales. More importantly, processes like low-cloud precipitation and cloud-top entrainment rate are difficult to measure, even during extensive field campaigns. This makes it hard to attempt observational correlations between cloud property changes and the processes that cause them. Several studies with cloud-resolving models (CRMs), however, have attempted to simulate the transition from stratocumulus to trade cumulus clouds in the Tropics by increasing the sea surface temperature underneath the clouds and documenting the changes in the resulting cloud field (e.g., Krueger et al. 1995; Wyant et al. 1997). They find a transition from a regime of horizontally extensive clouds with large water contents and small vertical extents over colder waters to a regime of vertically extensive clouds with small water contents over warmer waters. This transition is accompanied by an increase in the rate of precipitation as the sea surface temperature increases (Wyant et al. 1997). These results appear to agree with the behavior of the GCM's low clouds, even though it is not clear whether, in a statistical analysis of the CRM runs, the cloud water decreases with temperature would outweigh

the radiative effects of the DZ increases. Wyant et al. (1997) point out that, in their model, the role of cloud-top entrainment instability in the breakup of the stratocumulus cloud deck is secondary to the role of the decoupling of the cloud from the subcloud layer and the subsequent entrainment of dry above-inversion air caused by penetrating cumulus clouds. This process becomes more vigorous as the SST and the latent heat fluxes in the boundary layer increase, and is primarily responsible in the CRM runs for the LWC decreases over warmer waters.

Both the GCM and CRM simulations point to entrainment and precipitation as two processes that deplete cloud water with increasing efficiency as temperature increases. The GCM captures only the direct effect of those processes on the cloud water, whereas the CRMs incorporate additional indirect effects related to the decoupling of the cloud from the subcloud layer and to the action of penetrating convection. Those indirect effects are not resolved by the cloud parameterization employed in the GISS GCM. To this point, however, CRM simulations have emphasized only the subtropical stratocumulus-to-trade cumulus transition, with both cloud types present. The behavior found in the ISCCP observations and in the GCM simulation is more global in nature occurring throughout the deep Tropics and over warm land areas as well. A general parametric representation of entrainment dilution of cloud water in all conditions, with or without instability, does not currently exist. Analyses of FIRE data (Hanson 1991) indicate that marine stratus albedo changes of up to 50% are possible with only moderate changes in above-cloud humidity. The existing GCM parameterizations of cloud water evaporation should at least qualitatively capture this aspect of the physics controlling the optical thickness of such clouds.

Over land, cloud vertical extent in the model exerts a larger control over optical thickness at all latitudes than is the case for maritime clouds. However, we have examined only a January simulation in this paper; in the ISCCP data,  $d \ln(\text{TAU})/dT$  over land is positive in midlatitudes in winter but turns to strong negative in summer (Tselioudis and Rossow 1994). Thus, our conclusions about continental clouds are specific only to boreal winter and should be reexamined for summer conditions. We also note that there is a paucity of both observations and theoretical studies of continental low clouds, and so it remains to be seen whether ideas about marine stratus decks can be applied to continental stratus.

The doubled- $\text{CO}_2$  runs with the GISS GCM show that, in the model, current-climate changes of low cloud optical thickness are related to temperature variations strongly enough that they can be used to qualitatively predict the changes of optical thickness in a warmer climate. This raises the possibility that, in the real world, current-climate temperature transitions from optically thick stratocumulus decks to optically thinner broken

stratocumulus and trade cumulus clouds may translate into a decrease in the coverage of the former and an increase in the coverage of the latter as climate warms, allowing more sunlight to reach the surface in the tropical regions. The examination of the climate feedbacks produced by low cloud optical thickness changes in the GISS GCM showed that, whereas such changes have small effects on the model's global climate sensitivity, they influence strongly the latitudinal distribution of the greenhouse warming. The reduction in the high-latitude amplification of the warming affects the strength of the atmospheric circulation, which can feed back on the water vapor, the oceanic circulation, and finally the cloud field itself. It is important to note that the absence of an effect on global climate sensitivity is specific to the GISS GCM, which in its older version prescribed optical thickness as a decreasing function of altitude. For GCMs currently diagnosing LWC as a function of temperature, for example, using instantaneous condensation or the Betts and Harshvardhan (1987) prescription, substitution of a parameterization with cloud water dilution and variable thickness could produce a substantial increase in global sensitivity. Finally, we would like to emphasize that we have explored only one part of the cloud optical thickness feedback issue. Midlevel and high clouds are subject to different dynamic and thermodynamic influences and have different radiation forcing, primarily in the longwave.

This study demonstrates the validity of the use of GCMs to provide probable explanations for large-scale statistical relationships that are derived from the analysis of observational data. Such explanations can then be assessed through the use of observations more detailed and better tailored to the problem at hand. The study also illustrates that potential cloud feedbacks on climate are far more complicated than those predicted by simple adiabatic calculations, or by climate models using cloud schemes that rely on those calculations. The optical properties of the clouds are determined by a balance of water-forming and water-depleting processes that depend on dynamical, thermodynamical, and microphysical conditions. The inclusion of interactive optical properties in GCM cloud schemes constitutes a large step ahead in the effort to understand and resolve this balance: the older version of the GISS GCM cloud scheme produced changes of low cloud optical thickness with temperature that bear little resemblance to the observations. It is imperative, however, to continue the effort to transfer cloud processes included in cloud-resolving models to the GCM cloud scheme in order to increase our confidence in the cloud feedbacks produced by the climate models.

*Acknowledgments.* The authors wish to thank William Rossow for several helpful comments and suggestions. This research was supported by the NASA Program on Global Radiation Data Analysis and Modeling (managed by Dr. Robert J. Curran and Dr. Robert A. Schiffer),

the DOE Atmospheric Radiation Measurement Program, the First ISCCP Regional Experiment III Program, and the Tropical Rainfall Measuring Mission.

## REFERENCES

- Albrecht, B. A., M. P. Jensen, and W. J. Syrett, 1995: Marine boundary layer structure and fractional cloudiness. *J. Geophys. Res.*, **100**, 14 209–14 222.
- Betts, A. K., and Harshvardhan, 1987: Thermodynamic constraint on the cloud liquid water feedback in climate models. *J. Geophys. Res.*, **92**, 8483–8485.
- Blackmon, M. L., J. E. Geisler, and E. J. Pitcher, 1983: A general circulation model study of January anomaly patterns associated with interannual variation of equatorial Pacific sea surface temperatures. *J. Atmos. Sci.*, **40**, 1410–1425.
- Considine, G., J. A. Curry, and B. Wielicki, 1997: Modeling cloud fraction and horizontal variability in marine boundary layer clouds. *J. Geophys. Res.*, **102**, 13 517–13 525.
- Del Genio, A. D., and M.-S. Yao, 1993: Efficient cumulus parameterization for long-term climate studies: The GISS scheme. *The Representation of Cumulus Convection in Numerical Models, Meteor. Monogr.*, No. 46, Amer. Meteor. Soc., 181–184.
- , —, W. Kovari, and K.-W. Lo, 1996: A prognostic cloud water parameterization for global climate models. *J. Climate*, **9**, 270–304.
- Feigelson, E. M., 1978: Preliminary radiation model of a cloudy atmosphere. Part I: Structure of clouds and solar radiation. *Beitr. Phys. Atmos.*, **51**, 203–229.
- Fowler, L. D., D. A. Randall, and S. A. Rutledge, 1995: Liquid and ice cloud microphysics in the CSU general circulation model. Part I: Model description and simulated microphysical processes. *J. Climate*, **9**, 489–529.
- Greenwald, T. J., G. L. Stephens, S. A. Christopher, and T. H. Vonder Haar, 1995: Observations of the global characteristics and regional radiative effects of marine cloud liquid water. *J. Climate*, **8**, 2928–2946.
- Gultepe, I., G. A. Isaac, W. R. Leaitch, and C. M. Banic, 1996: Parameterizations of marine stratus microphysics based on in situ observations: Implications for GCMs. *J. Climate*, **9**, 345–357.
- Hansen, J. E., and L. D. Travis, 1974: Light scattering in planetary atmospheres. *Space Sci. Rev.*, **16**, 527–610.
- , G. Russel, D. Rind, P. Stone, A. Lacis, S. Lebedeff, R. Ruedy, and L. Travis, 1983: Efficient three-dimensional global models for climate studies: Models I and II. *Mon. Wea. Rev.*, **111**, 609–662.
- , A. Lacis, D. Rind, G. Russell, P. Stone, I. Fung, R. Ruedy, and J. Lerner, 1984: Climate sensitivity: Analysis of feedback mechanisms. *Climate Processes and Climate Sensitivity, Geophys. Monogr.*, No. 29, Amer. Geophys. Union, 130–163.
- Hanson, H. P., 1991: Cloud albedo control by cloud-top entrainment. *Tellus*, **43A**, 37–48.
- Hartke, G. J., and D. Rind, 1997: Improved surface and boundary layer models for the Goddard Institute for Space Studies general circulation model. *J. Geophys. Res.*, **102**, 16 407–16 422.
- Klein, S. A., and D. L. Hartmann, 1993: The seasonal cycle of low stratiform clouds. *J. Climate*, **6**, 1587–1606.
- Krueger, S. K., G. T. McLean, and Q. Fu, 1995: Numerical simulation of the stratus-to-cumulus transition in the subtropical marine boundary layer. Part II: Boundary-layer circulation. *J. Atmos. Sci.*, **52**, 2851–2868.
- Le Treut, H., and Z.-X. Li, 1991: Sensitivity of an atmospheric general circulation model to prescribed SST changes: Feedback effects associated with the simulation of cloud optical properties. *Climate Dyn.*, **5**, 175–187.
- Li, Z.-X., and H. LeTreut, 1992: Cloud-radiation feedbacks in a general circulation model and their dependence on cloud modeling assumptions. *Climate Dyn.*, **7**, 133–139.
- MacVean, M. K., and P. J. Mason, 1990: Cloud-top entrainment instability through small-scale mixing and its parameterization in numerical models. *J. Atmos. Sci.*, **47**, 1012–1030.
- Mitchell, J. F. B., C. A. Senior, and W. J. Ingram, 1989: CO<sub>2</sub> and climate: A missing feedback? *Nature*, **341**, 132–134.
- Randall, D. A., 1980: Conditional instability of the first kind upside-down. *J. Atmos. Sci.*, **37**, 125–130.
- Roeckner, E., 1988: Negative or positive cloud optical depth feedback? *Nature*, **335**, 304.
- Rossow, W. B., and R. A. Schiffer, 1991: ISCCP cloud data products. *Bull. Amer. Meteor. Soc.*, **72**, 2–20.
- Smith, R. N. B., 1990: A scheme for predicting layer clouds and their water content in a general circulation model. *Quart. J. Roy. Meteor. Soc.*, **116**, 833–856.
- Sundqvist, H., 1978: A parameterization scheme for non-convective condensation including prediction of cloud water content. *Quart. J. Roy. Meteor. Soc.*, **104**, 677–690.
- , E. Berge, and J. E. Kristjansson, 1989: Condensation and cloud parameterization studies with a mesoscale numerical weather prediction model. *Mon. Wea. Rev.*, **117**, 1641–1657.
- Tselioudis, G., and W. B. Rossow, 1994: Global, multiyear variations of optical thickness with temperature in low and cirrus clouds. *Geophys. Res. Lett.*, **21**, 2211–2214.
- , —, and D. Rind, 1992: Global patterns of cloud optical thickness variation with temperature. *J. Climate*, **5**, 1484–1495.
- , A. A. Lacis, D. Rind, and W. B. Rossow, 1993: Potential effects of cloud optical thickness on climate warming. *Nature*, **366**, 670–672.
- Walcek, C. J., 1994: Cloud cover and its relationship to relative humidity during a springtime midlatitude cyclone. *Mon. Wea. Rev.*, **122**, 1021–1035.
- Washington, W. M., and G. A. Meehl, 1984: Seasonal cycle experiments on the climate sensitivity due to a doubling of CO<sub>2</sub> with an atmospheric general circulation model coupled to a simple mixed layer ocean model. *J. Geophys. Res.*, **89** (D6), 9475–9503.
- Wetherald, R. T., and S. Manabe, 1986: An investigation of cloud cover change in response to thermal forcing. *Climate Change*, **8**, 5–23.
- Wyant, M. C., C. S. Bretherton, H. A. Rand, and D. E. Stephens, 1997: Numerical simulations and a conceptual model of the stratus-to-cumulus transition. *J. Atmos. Sci.*, **54**, 168–192.
- Xu, K.-M., and S. K. Krueger, 1991: Evaluations of cloudiness parameterizations using a cumulus ensemble model. *Mon. Wea. Rev.*, **119**, 342–367.